Proceedings of the International Conference on Heat Exchanger Fouling and Cleaning - 2024 (Peer-reviewed)
April 21–26, 2024, Lisbon, Portugal; Editors: H.U. Zettler and E.M. Ishiyama

NUMERICAL MODEL FOR THE CLEANING OF A FILM-LIKE SOIL BY VISCOUS SHIFTING UNDER NON-ISOTHERMAL CONDITIONS

***C. Golla[1], V. Liebmann[1], R. Rebel[1], H. Köhler[2], J. Fröhlich[1] and F. Rüdiger[1]**
[1] Institute of Fluid Mechanics, Technische Universität Dresden, Germany, christian.golla@tu-dresden.de
[2] Institute of Natural Materials Technology, Technische Universität Dresden, Germany

ABSTRACT

Predicting the cleaning time of a fouling layer, termed *soil*, is the subject of current research. One approach to tackle this problem for film-like soils is the identification of different, prototypical modes of removal, called *cleaning mechanisms*. This allows employment of dedicated modeling approaches for each of the cleaning mechanisms. In the present paper, a model for the cleaning mechanism *viscous shifting* is presented.

Existing approaches to model viscous shifting soils are reviewed. Compared to the existing models, the new model proposed here has three distinctive features: i) geometry-independent formulation for a range of geometries, ii) decoupling of flow computation and soil removal, iii) consideration of non-isothermal scenarios. The model is validated based on two representative cases: jet cleaning of a Newtonian oil layer and a flushing process of chocolates. In the latter also a non-isothermal scenario is considered. The presented model is able to capture the evolution of soil height over time for all cases investigated. The present model achieves relative.

INTRODUCTION

In various industrial settings, machines and equipment must be cleaned between processes so that no residuals remain adhering to the surface [1]. The problems resulting from even very thin layers of fouling, termed *film-like soil* here, vary depending on the industry. While it constitutes a risk of cross-contamination and consumer safety in the food processing or the pharmaceutical industry, it causes a loss of heat transfer efficiency in crude oil processing [2], for example. Hence, ongoing research aims to obtain models that predict the cleaning time of film like soil layers [3]. There exist rules of thumb, like requiring flow velocities of at least $1.5\,\mathrm{m/s}$ for cleaning pipes [3]. These might provide sufficient cleaning, but far more resources are used than necessary [4, 5]. This includes energy, chemicals, water [6] and results in longer times required for cleaning.

A virtual systematic variation of cleaning parameters can be performed to optimize the process by simulating cleaning processes [7]. Fully resolved simulations of cleaning can be undertaken for simple configurations but are very expensive. An efficient and practically preferable alternative is provided by *boundary condition cleaning models* (BCCM), first introduced in [8]. In a BCCM, the fluid flow is computed using computational fluid dynamics (CFD) without considering the dimensions of the film-like soil. In a second step, the removal of the soil itself is computed while the flow field is kept frozen. The underlying concept is to use different BCCMs according to how a soil reacts when subjected to a specific cleaning procedure. This type of reaction is termed *cleaning mechanism* [9]. The cleaning mechanisms distinguished in the present framework were defined by Köhler et al. [10]: *cohesive separation* [11], *adhesive detachment* [7, 12], *viscous shifting*, and *diffusive dissolution* [8, 13–15]. Other authors [16–19] use slightly different versions of the cleaning mechanisms, with [20] providing a detailed review. The present work aims to develop a new BCCM for viscous shifting. In the case of viscous shifting, the applied loads cause the soil to flow, often with instability of the interface between the soil and the outer liquid.

Before doing so, existing models addressing viscous shifting in context with cleaning of film-like soils are reviewed. Flushing or, synonymously, purging of pipes and jet cleaning of surfaces are well-investigated scenarios where viscous shifting appears. In the case of flushing processes, i.e., the displacement of the previous liquid by a following liquid, authors [3, 16, 21, 22] typically distinguish between two different stages of: The *core removal* phase in which the soil is removed from the center of the pipe. In this stage, removal is mainly caused by forces arising from pressure gradients. And the *layer removal* phase, in which a thin residual layer of soil is removed from the wall. Here, the removal of the residual layer is driven by shear forces [21]. Core removal is not addressed in the present work since the soil is not film-like during this phase. Details and modeling approaches can be found in [23–29]. Palabiyik et al. [3] mention a third possible phase called *patch removal*. In this phase, the continuous soil layer breaks into patches that erode. In this phase cleaning mechanisms other than viscous shifting might also be active. For layer

ISBN: 978-0-9984188-3-4; Published online www.heatexchanger-fouling.com

Table 1. Comparison of different models for viscous shifting of film-like soils. P – Pipe, J – Jet.

Model	**Mickaily** [1]	**Yan** [30]	**Liebmann** [31]	**Fernandes** [32]	**Yeckel** [36]	**Fernandes** [35]	**Present work**
Applied to	P	P	P	P	J	J	P, J
Decoupling flow – soil	✓	✓	-	✓	✓	✓	✓
Spatially resolved	-	✓	-	-	✓	✓	✓
Non-Newtonian	-	-	✓	✓	-	✓	✓
Non-isothermal	-	-	-	-	-	-	✓
Instabilities	-	-	-	-	-	-	-

removal, different models exist. The first one was presented by Mickaily and Middleman [1]. The starting point of this model is a local mass balance of the residual soil layer, which yields an evolution equation for the soil height in space and time. The equation was solved analytically for the spatially averaged soil film height in a pipe. The model, however, contains an empirical constant, which must be determined experimentally before quantitative agreement is achieved. Later, Yan et al. [30] proposed an extension where the evolution equation for the soil height was solved using the method of characteristics without spatial averaging. This model does not require empirical correction. Liebmann et al. [31] presented a combined model for both cleaning phases addressing non-Newtonian fluids under the assumption of laminar pipe flow. The layer removal model part assumes a linear velocity profile in the soil layer, and a modified analytical solution for the main fluid is employed. Fernandes et al. [32] investigated removal of toothpaste from pipes using water. During this process, the fluids are arranged concentrically with water inside. Here, two types of removal might occur: Shear-driven removal, reported below, and mass transfer. When describing the shear-driven removal, the change of mass over time is modeled. The change of mass is assumed to be proportional to the soil density, the interface area, the maximum velocity of water in the core of the pipe and the ratio between the interfacial shear stress and a critical stress. The results are compared to the measurements of Palabiyik et al. [3] and match their observations.

Similar classifications were introduced for jet cleaning. Fernandes et al. [33–35] identified three regimes of soil cleaning, depending on the relative thickness of the soil layer: i) *very thin layers*, where the soil height h_s is much smaller than the height of the cleaning fluid film h_{fi}, so that the removal is mainly shear driven [35, 36], ii) *thin layers*, where $h_s \approx h_{fi}$ with the removal being driven mainly by momentum [33–35, 37], iii) *thick layers*, where $h_s > h_{fi}$, so that the mechanisms at work are more complex [38]. Relevant for the present work are only very thin layers. In the model of Yeckel and Middleman [36] the dimensions of the soil are neglected, and radial pressure and shear stress distributions are obtained from analytical solutions for the single-phase flow. These distributions are used as boundary conditions for Stokes equations [39], describing the soil flow. Subsequently, the authors presented extensions accounting for grooved surfaces [40] and problems without neglecting the soil dimensions when calculating the jet flow [41]. Fernandes et al. [35] later extended the Yeckel and Middleman model towards non-Newtonian fluids, which requires to solve the resulting partial differential equations numerically. An overview of the features of the different models is provided in Tab. 1.

The BCCM presented in the present work accounts for non-Newtonian fluids and for temperature-dependent soil viscosity. Additionally, the formulation of the model is not specific for one configuration. Validation will be performed on both jet cleaning of an oil layer and layer removal in a flushing process of chocolates. In the latter, insulated pipes are typically used to temper the chocolate. For this case a thermal sub-model is developed. None of the models presented in the literature include a thermal sub-model. However, the model will not account for interfacial instabilities. It is expected to work nevertheless, since authors of previous models [1, 30] also neglected instabilities in their model formulations and the model results were in agreement with their validation experiments, within which instabilities were observed. In [1], a wavelike pattern was observed, which moved at a rate consistent with the flushing fluid. It was concluded that the global movement of the film is well estimated using the wall shear stress of the flushing fluid flowing

ISBN: 978-0-9984188-3-4; Published online www.heatexchanger-fouling.com

through a pipe without a soil film. However, this may no longer be the case with gas-liquid system

MODELING OF VISCOUS SHIFTING

Model overview

The model is developed as a BCCM, which implies the standard assumptions for all BCCMs [7, 11].

1. The height of the soil is negligible compared to the dimensions of the flow. Hence, the cleaning fluid's flow is computed without considering the soil.
2. The cleaning progress does not influence the fluid forces acting on the soil
3. The height of the soil is negligible compared to the soil length ($h_s \ll L_s$). With that, transport processes into the soil, e.g., swelling and heating, can be described using one-dimensional transport equations using the wall-normal direction.

Further assumptions will be made during the model description. For modeling, the process of viscous shifting is divided into the four subprocesses shown in Fig. 1. In the first step, the loads acting on the soil are calculated using a comparative stress τ_{hyd}. In the second step, the thermal behavior of the soil is modeled. This is an important aspect of viscous shifting, as temperature has a strong influence on the viscosity of most soils. In the third step the soil rheology needs to be evaluated, which in general has the form $\tau_s = f(\dot{\gamma}_s, \vartheta_s)$. Here, τ_s is the shear stress present in the soil, $\dot{\gamma}_s$ the shear rate of the soil and ϑ_s is the soil temperature. In the final step, the computed quantities are combined to determine the movement of the soil. In the following sections, the modeling of the soil movement is discussed in detail, before modeling the thermal behavior.

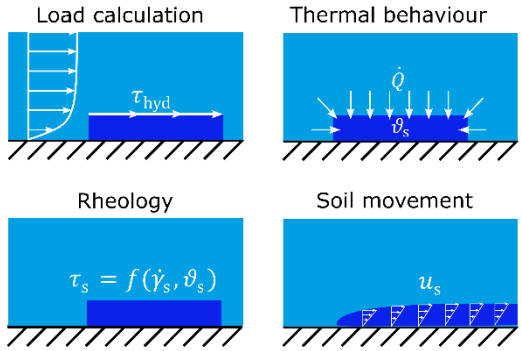

Fig. 1. Decomposition of viscous shifting in subprocesses for the modeling (graph after [7, 11]).

Load calculation

The mechanical load acting on the soil must be determined. As a consequence of BCCM assumption 1, the fluid flow can be determined from a single-phase flow investigation. To make this clearer, two views are introduced in Fig. 2. The single-phase view is used for flow calculation. In that case, the x-y-coordinates are used without subscripts. The multiphase view is used for model description and accounts for the actual dimensions of the soil. In that case, the x_s-y_s –coordinates are used. There are different ways possible to obtain a single-phase flow solution: experimental measurements or CFD simulations. If available, even analytical solutions can be employed.

In a general flow situation, a combination of pressure and shear forces is acting on the soil. The present approach will be limited to shear forces since the height of the soil is assumed to be small, and thus, the side areas where the pressure force could attack are very small and hence negligible compared to the shear forces acting on top of the soil. However, there may be scenarios in which pressure forces become relevant even in the case of film-like soils. Examples are if negative pressure, pressure oscillation, or cavitation are used for cleaning. These situations are not considered in the modeling. Even if only shear forces are considered, the general fluid stress tensor $\boldsymbol{\tau}$ consists of 6 independent components. To obtain a scalar reference value τ_{hyd}, the magnitude of the wall shear stress is integrated across the soil-cleaning fluid interface, A_{int}. This yields

$$\tau_{\mathrm{hyd}} = \int_{A_{\mathrm{int}}} \|\boldsymbol{\tau} \cdot \boldsymbol{n}\| \, \mathrm{d}A. \qquad (1)$$

The magnitude is used so that opposing shear stresses do not compensate each other during the averaging procedure. In cases where pressure forces are more relevant, they must be included in the calculation of the comparative stress τ_{hyd}.

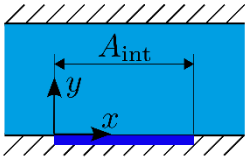

a) Single-phase view for flow computation

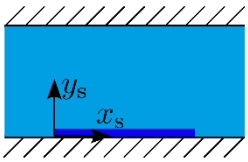

b) Multi-phase view for soil modeling

Fig. 2. Different views for flow computation and soil modeling.

ISBN: 978-0-9984188-3-4; Published online www.heatexchanger-fouling.com

Modeling of soil movement

For modeling of the soil movement, the soil is discretized in flow direction into N_{seg} segments. The discretization is depicted in Fig. 3. Only the flow component in the main flow direction is considered. The soil layer is assumed to be very thin. Therefore, the velocity profile in each segment i, is approximated with a linear function reading

$$u_{\mathrm{s},i}(y_{\mathrm{s}}) = \dot{\gamma}_{\mathrm{s},i} y_{\mathrm{s}}, \tag{2}$$

where $\dot{\gamma}_{\mathrm{s},i}$ is the shear rate and y_{s} the wall normal coordinate. This simplification is not valid if the soil layer height is too large or effects like wall slip become dominating. At the interface of the soil layer and cleaning fluid, the normal stresses are assumed to be in balance. Assuming the soil rheology of the form $\tau_{\mathrm{s}} = f(\dot{\gamma}_{\mathrm{s}}, \vartheta_{\mathrm{s}})$, the shear rate is determined by inserting the comparative stress in the rheology law and solving for $\dot{\gamma}_{\mathrm{s},i}$.

$$\tau_{\mathrm{hyd},i} = \tau_{\mathrm{s}} = f(\dot{\gamma}_{\mathrm{s},i}, \vartheta_{\mathrm{s},i}) \tag{3}$$

The computation of the soil temperature $\vartheta_{\mathrm{s},i}$ is discussed in the following section. Since the velocity profile is known, it can be integrated over the cross-section area $A_{\mathrm{out},i}$ to obtain the mass flow leaving a segment

$$\dot{m}_{\mathrm{s,out},i} = \rho_{\mathrm{s}} \int_{A_{\mathrm{out},i}} u_{\mathrm{s},i} \, \mathrm{d}A. \tag{4}$$

Herein, ρ_{s} is the soil density, and $S_{\mathrm{out},i}$ is the surface area of the outlet of cell i. The incoming mass flow in a segment is assumed to be the mass flow leaving the segment directly upstream, i.e.

$$\dot{m}_{\mathrm{s,in},i} = \begin{cases} 0 & i = 1, \\ \dot{m}_{\mathrm{s,out},i-1} & \text{else.} \end{cases} \tag{5}$$

The change of mass in a segment can be expressed by

$$\frac{\mathrm{d}m_{\mathrm{s},i}}{\mathrm{d}t} = \dot{m}_{\mathrm{s,out},i} - \dot{m}_{\mathrm{s,in},i}. \tag{6}$$

Equation (5) is discretized using the Euler forward method, yielding

$$m_{\mathrm{s},i}^{(n+1)} = m_{\mathrm{s},i}^{(n)} - \Delta t \left(\dot{m}_{\mathrm{s,out},i}^{(n)} - \dot{m}_{\mathrm{s,in},i}^{(n)} \right), \tag{7}$$

where Δt is the time step size and the superscript (n) refers to the approximation of a quantity at time $t^{(n)} = n\Delta t$. The way Eq. (6) is discretized imposes a stability criterion. It must be ensured that the mass within a segment is always larger than the mass being removed by Eq. (7). This causes the segments to never be completely empty, i.e., clean. One way to overcome this issue is to define a critical soil height where a segment is considered to be clean. The numerical value of this threshold needs to be defined problem specific. Another workaround would be the combination with the model for adhesive detachment [7, 12], which would define a physical criterion for the detachment of the soil from the substrate. A combination of both models will be presented in [42].

The way the mass of the soil segment $m_{\mathrm{s},i}$ is related to the segment height $h_{\mathrm{s},i}$, as well as the bounding areas of the segments $A_{\mathrm{top},i}$ and $A_{\mathrm{out},i}$, depends on the investigated geometries and will be provided below, with the description of the test cases. Throughout the derivation, a unique flow direction was assumed. This is not met in all practical applications. However, the assumption does not constitute a major restriction since a more general formulation involving the flow direction can be derived using the concept of fluxes known from finite volume methods and is part of future work.

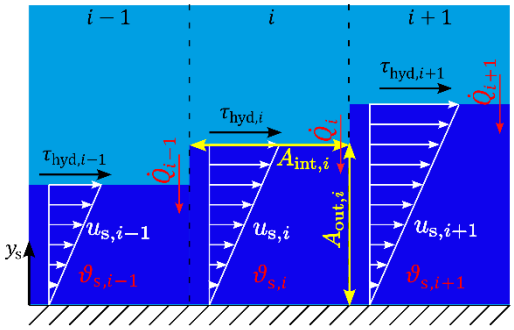

Fig. 3. Sketch of the discretization of the soil into segments. All quantities are defined in the text.

Thermal modeling

The aim of this section is to derive equations that can be used to compute the evolution of the soil temperature over time. The thermal model is designed for application to the flushing processes of chocolate, where insulated pipes are used. Hence, the walls are assumed to be adiabatic. The temperature in each soil segment is assumed to be uniform. The initial phase with a non-uniform temperature profile is neglected in the present framework. A more general approach accounting for non-uniform temperature distributions and non-adiabatic walls will be provided in [42].

The enthalpy stored in each segment can be written as

$$H_{\mathrm{s},i} = m_{\mathrm{s},i} c_{p,\mathrm{s}} \vartheta_{\mathrm{s},i}, \tag{8}$$

where $c_{p,\mathrm{s}}$ is the heat capacity of the soil. Equation (8) implicitly assumes a reference state of $\vartheta_{\mathrm{ref}} = 0\ °\mathrm{C}$.

When the soil is moving, convective enthalpy transport occurs, which can be computed analogously to Eq. (7) as

$$\tilde{H}_{\mathrm{s},i}^{(n+1)} = H_{\mathrm{s},i}^{n} - \Delta t \left(\dot{H}_{\mathrm{s,out},i}^{(n)} - \dot{H}_{\mathrm{s,in},i}^{(n)} \right), \tag{9}$$

ISBN: 978-0-9984188-3-4; Published online www.heatexchanger-fouling.com

where $\tilde{H}_{\mathrm{s},i}^{n+1}$ is an intermediate value for the thermal energy since it does not account for heat convection from the main flow, yet. The enthalpy fluxes in Eq. (9) are computed as

$$\dot{H}_{\mathrm{s,out},i} = \dot{m}_{\mathrm{s,out},i} c_{p,\mathrm{s}} \vartheta_{\mathrm{s},i}, \tag{10}$$

and

$$\dot{H}_{\mathrm{s,in},i} = \begin{cases} 0 & i = 1 \\ \dot{H}_{\mathrm{s,out},i-1} & \text{else.} \end{cases} \tag{11}$$

Furthermore, heat can be transported via convection from the bulk flow into the soil as according to

$$\dot{Q}_i = h_{\vartheta,i} A_{\mathrm{int},i} (\vartheta_{\mathrm{f}} - \vartheta_{\mathrm{s},i}), \tag{12}$$

where $h_{\vartheta,i}$ is the heat transfer coefficient of segment i. It must be determined individually for the problem at hand. The temperature of the bulk flow, ϑ_{f}, is assumed to be constant, since the mass of soil acting as heat sink or source is small. The enthalpy is updated using

$$H_{\mathrm{s},i}^{(n)} = \tilde{H}_{\mathrm{s},i}^{(n)} + \Delta t \dot{Q}_i^{(n)}. \tag{13}$$

Computational algorithm

Assuming that hydrodynamic loads $\tau_{\mathrm{hyd},i}$ (Eq. (1)), initial masses $m_{\mathrm{s},i}^0$ and enthalpies $H_{\mathrm{s},i}^0$, are known, the following steps are computed within each time step:

1. Compute soil heights $h_{\mathrm{s},i}^{(n)}$ and temperatures $\vartheta_{\mathrm{s},i}^n$ from masses and energies.
2. Compute the shear rates $\dot{\gamma}_{\mathrm{s},i}^{(n)}$ (Eq. (3)) and the velocity profiles $u_{\mathrm{s},i}^{(n)}(y)$ (Eq. (2)).
3. Propagate the mass to the next timestep using Eq. (4, 5) and (7).
4. Propagate the enthalpy to the next timestep using Eq. (9-11).
5. Account for thermal energy transported by convection from the bulk flow into the soil using Eq. (12, 13).

If the investigated case is isothermal, the shear rates $\dot{\gamma}_{\mathrm{s},i}^{(n)}$ do not vary over time. Consequently, the shear rate only needs to be computed once at the beginning. Additionally, in an isothermal case steps 4 and 5 are not necessary.

FLUSHING IN AN ISOTHERMAL PIPE

Setup

As a first validation, flushing processes of chocolates in a straight pipe under isothermal conditions at temperatures of $\vartheta \in \{40, 52\}$ ℃ are investigated. The setup was taken from Liebmann et al. [21]. The authors performed simulations of the flushing process using the volume of fluid (VOF) method from the CFD library OpenFOAM. The setup is depicted in Fig. 4. It features a pipe of length $L = 1$ m and radius $R = 13$ mm, which is initially entirely filled with white chocolate. During the flushing process, dark chocolate pushes out the white chocolate. Applying the present wording, white chocolate corresponds to the soil, and dark chocolate to the cleaning fluid. The rheology of both fluids is described using the Windhab model [43], reading

$$\tau_{\mathrm{s}}(\dot{\gamma}) = \tau_0 + (\tau_1 - \tau_0)\left(1 - \exp\left(-\frac{\dot{\gamma}}{\dot{\gamma}_{\mathrm{ref}}}\right)\right) + \eta_\infty \dot{\gamma}. \tag{14}$$

The rheological parameters $\tau_0, \tau_1, \dot{\gamma}_{\mathrm{ref}}, \eta_\infty$ are temperature dependent. Their dependency is modelled using an exponential ansatz $P(\vartheta) = B_{P,1} \exp\left(B_{P,2}/(\vartheta - B_{P,3})\right)$, where P stands for the respective parameter. Values for the constants $B_{P,1}, B_{P,2}$ and $B_{P,3}$ can be found in the original work [21]. The density of the white chocolate is $\rho_{\mathrm{s}} = 1200\ \mathrm{kg/m^3}$ and the density of the dark chocolate is $\rho_{\mathrm{f}} = 1260\ \mathrm{kg/m^3}$ In the simulation, the pipe flow is driven by a pressure gradient so adjusted such that the bulk velocity of the flow is $u_{\mathrm{b}} = 0.1\ \mathrm{m/s}$.

To synthesize suitable initial conditions for the present framework, the height of the soil layer h_{s} was determined from the simulations by evaluating

$$h_{\mathrm{s}}(x,t) = R - \sqrt{\frac{1}{\pi}\int_{A_{\mathrm{av}}(x)} \alpha(x,y,z)\mathrm{d}A}, \tag{15}$$

where α is the phase indicator being equal to 1 in the cleaning fluid and 0 in the soil. The second term in Eq. (15) is the equivalent radius of the area occupied by the cleaning fluid [21] and the integration was performed over cross-sections of the pipe, depicted in Fig. 3. A limit $h_{\mathrm{s,max}}$ was defined, for which the remaining layer of soil was sufficiently small to fulfill the assumptions of the present model. The first time, where $\forall x: h_{\mathrm{s}}(x,t) \leq h_{\mathrm{s,max}}$ was considered as starting time t_{st} for simulation using the present model. Subsequently, the pipe was discretized in N_{seg} equally sized segments of length $L_{\mathrm{seg}} = L/N_{\mathrm{seg}}$. and in each segment the soil height was averaged to obtain initial values of the soil thickness in each segment, $h_{\mathrm{s},i}^{(0)}$.

The flow of the cleaning fluid was computed without consideration of the soil as discussed above. For the present case, this results in computing the developed single-phase flow of a Windhab fluid in a straight pipe. The analytical solution [21, 44] is employed to obtain the shear stress acting on the soil. Within the model framework, the domain occupied with soil corresponds to hollow cylinders where the areas depicted in Fig. 3 are defined as $A_{\mathrm{out},i} = \pi\left(R^2 - \left(R - h_{\mathrm{s},i}\right)^2\right)$, $A_{\mathrm{int},i} = 2\pi(R -$

ISBN: 978-0-9984188-3-4; Published online www.heatexchanger-fouling.com

$h_{s,i})L_{seg}$. The mass of each segment is computed as $m_{s,i} = \rho_s A_{out,i} L_{seg}$.

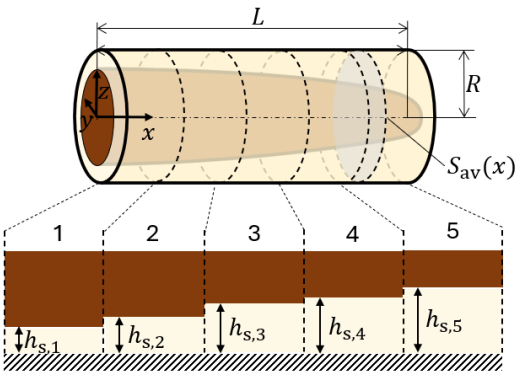

Fig. 4. Investigated pipe flow. Discretization is shown for $N_{seg} = 5$. Not drawn to scale.

Results

Figure 5 displays the evolution of the soil height $h_{s,i}$ in the segments over time for $\vartheta_f = \vartheta_s = 40$ °C. The relative differences between the soil height from the present simulations and the reference case are depicted in Fig. 6 for $\vartheta = 40$ °C and in Fig. 7 for $\vartheta_f = \vartheta_s = 52$ °C. The settings of the present model were $N_{seg} = 5$, $\Delta t = 0.1$ s and the numbering of the segments is according to Fig. 4. Applying the value of $h_{s,max} = 0.1R$ yields $t_{st} = 16.2$ s.

In case of $\vartheta = 40$ °C in segments $2, 3, 4$ and 5, the model matches the OpenFOAM data. The finest cell near the wall used in the OpenFOAM simulations has a radial expansion of $\Delta r/R = 0.01$. Hence, the values below $h_{s,i}/R = 0.01$ from the OpenFOAM simulation should be considered critically and cannot be employed for reasonable comparison. The reference simulation [21] for segment 5 shows some slight oscillations, indicating instabilities. Such instabilities are well-studied in the literature for core annular flows in straight pipes [45–49]. Following the discussion of Hu and Joseph [49], there are three kinds of interfacial instabilities: i) interfacial tension or capillary instabilities, which are dominant at very low Reynolds numbers, ii) interfacial friction instabilities, caused by viscosity differences of the two fluids, dominant at low Reynolds numbers and iii) Reynolds stress instabilities, caused by turbulence production in the bulk flow. Since surface tension was neglected and the Reynolds number is very small, these have to be interfacial friction instabilities. The cause of the instabilities may also be numerical. However, this has not yet been researched further and is beyond the scope of the present paper. The model at hand does not account for instabilities at all. However, the influence on the present results is negligible, and errors caused by this effect are minor. While the OpenFOAM simulation used as a reference case took around 20 h of computational time on 16 cores (AMD EPYC 7542 32-Core 2.9 GHz), the simulation with the present model took 0.2 s on 4 cores (Intel Core i5-6300, 2.4 GHz).

To obtain a single scalar value for the model performance, the relative root-mean-square error ε_{rms} was computed. This was done by comparing the height of the soil layer $h_{s,i}$ between the present simulation and the reference in each time step and averaging over the duration of the simulation, excluding values, where $h_{s,i,OF}/R < 0.01$. The error was normalized with the respective reference values $h_{s,i,OF}$.

Different timesteps Δt were investigated while holding the number of segments constant at $N_{seg} = 5$. The influence on the error was low if the stability criterion was fulfilled. The errors observed were around 6%. The influence of the number of segments is shown in Fig. 8. The error is around 25% for $N_{seg} = 1$ and decreases towards a minimum value of 6% at $N_{seg} = 5$. The error increases again for $N_{seg} > 5$. With a finer discretization, the local effect of interface instabilities on the soil height becomes more dominant.

The results obtained for $\vartheta = 52$ °C are similar so only the difference between the present results and the reference is shown in Fig. 7. The cleaning is faster, and the effect of the instability seems more dominant in segment 5, but still negligible. While the minimum ε_{rms} error of 9% is slightly higher compared to the $\vartheta = 40$ °C case, the dependency of the error on the time step and the number of segments observed are the same.

FLUSHING IN A NON-ISOTHERMAL PIPE

Setup

A non-isothermal case from Liebmann et al. [21] is investigated to validate the thermal modeling. The configuration is almost the same as described in the previous section. But here, the temperature is not constant anymore and the walls are considered to be adiabatic. Instead, the soil is initially at 40 °C, while the cleaning fluid enters the domain at 52 °C. The thermal conductivity κ of both fluids is assumed equal with $\kappa = 0.3$ W/(m K) [21]. Since the heat capacity varies only slightly with temperature, a constant value is assumed, with $c_{p,s} = 1560$ J/(kg K).

Additionally, the model requires a value for the heat transfer coefficient h_ϑ, which is determined from the Nusselt number $Nu = (h_\vartheta L_{chr})/\kappa$. Chocolate is a highly viscous fluid, and the flow velocity is low, which means the flow is laminar. Therefore, a Nusselt number of $Nu = 4.36$ is assumed, which is in the value for a laminar developed pipe flow of a Newtonian fluid with constant heat flux on the walls [50]. Note that this approach does not account for developing a thermal boundary layer. This would be of particular

ISBN: 978-0-9984188-3-4; Published online www.heatexchanger-fouling.com

importance in cases where an accurate prediction of a moving cleaning front is required. The characteristic length is $L_{\mathrm{chr}} = 2R$ in case of a pipe flow.

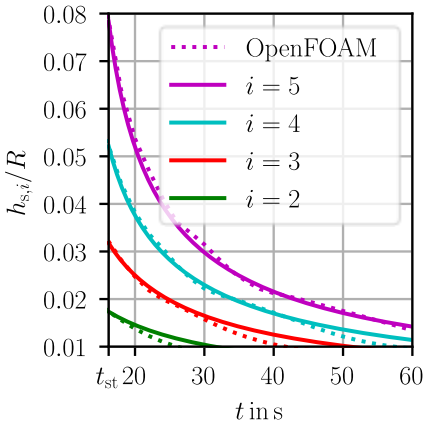

Fig. 5. Comparison of present results to the corresponding resolved OpenFOAM simulation from [21] in terms of evolution of soil height $h_{\mathrm{s},i}$ over time for $\vartheta = 40\ ^{\circ}\mathrm{C}$, $t_{\mathrm{st}} = 16.2$ s. Lines are only drawn where $h_{\mathrm{s},i,\mathrm{OF}}/R > 0.01$.

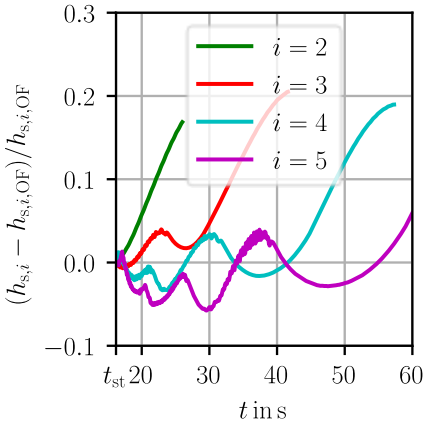

Fig. 6. Relative difference between present model and the corresponding resolved OpenFOAM simulation from [21] in terms of evolution of soil height $h_{\mathrm{s},i}$ over time for $\vartheta = 40\ ^{\circ}\mathrm{C}$, $t_{\mathrm{st}} = 16.2$ s. Lines are only drawn where $h_{\mathrm{s},i,\mathrm{OF}}/R > 0.01$.

The initial condition for the soil height in each segment is determined the same way as in the previous section. However, an additional initial condition for the soil temperature is required here. It is obtained by averaging the temperature within the soil segments at t_{st}. For the validation simulation, it is assumed that the temperature of the flushing fluid remains constant at $\vartheta_{\mathrm{f}} = 52\ ^{\circ}\mathrm{C}$ throughout the process.

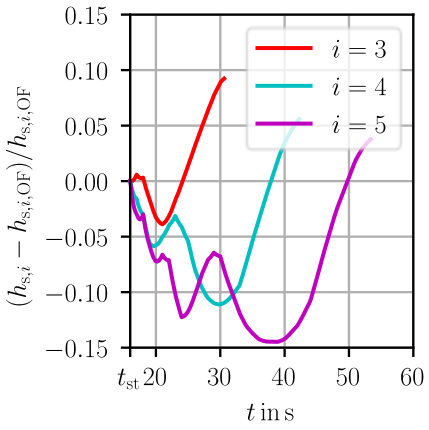

Fig. 7. Relative difference between present model and a resolved OpenFOAM simulation from [21] in terms of evolution of soil height $h_{\mathrm{s},i}$ over time for $\vartheta = 52\ ^{\circ}\mathrm{C}$, $t_{\mathrm{st}} = 16.0$ s. Lines are only drawn where $h_{\mathrm{s},i,\mathrm{OF}}/R > 0.01$.

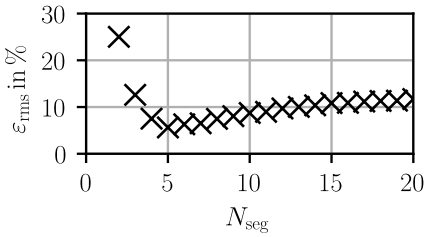

Fig. 8. Relative root-mean-square error $\varepsilon_{\mathrm{rms}}$ over number of segments for $\vartheta = 40\ ^{\circ}\mathrm{C}$.

Results

The simulations with the present model were repeated with the same discretization as above ($N_{\mathrm{seg}} = 5$, $\Delta t = 0.1$ s, $h_{\mathrm{s,max}} = 0.1R$ and $t_{\mathrm{st}} = 19.0$ s) for the non-isothermal case. Fig. 9 shows the relative difference in soil height, and Fig. 10 shows ~~in~~ the evolution of the soil temperature. Again, the present model matches the simulation results and the relative root-mean-square error $\varepsilon_{\mathrm{rms}}$ in terms of soil height is 6%, while it is 1% for the temperature. The present validation shows that the model can account for the temperature variation.

The presented part of the OpenFOAM simulation took 22 h on 16 cores (AMD EPYC 7542 32-Core 2.9 GHz), the simulation with the present model took 0.3 s on 4 cores (Intel Core i5-6300, 2.4 GHz), which is still negligible. However, it is worth noting that the thermal sub-model causes an increase of the duration by 50%, which could become crucial in more complex cases. The main reason for this increase is step 2 of the algorithm listed above. Adding the thermal sub-model makes it necessary to recompute the shear-rates $\dot{\gamma}_{\mathrm{s},i}^{n}$ using Eq. (3) in each time step. In the present case, the Windhab model, used to describe the soil rheology, cannot be

ISBN: 978-0-9984188-3-4; Published online www.heatexchanger-fouling.com

inverted analytically. Hence, a comparably expensive iterative procedure is required to solve it numerically. The numerical procedure is, however, is only necessary in case the law describing the rheology is not invertible.

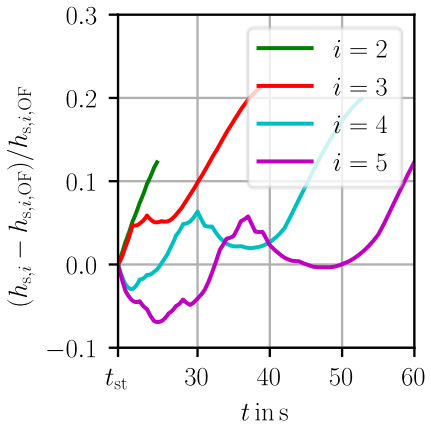

Fig. 9. Relative difference between present model and a resolved OpenFOAM simulation from [21] in terms of evolution of soil height $h_{s,i}$ over time under non-isothermal conditions, $t_{st} = 19.0$ s. Lines are only drawn where $h_{s,i,OF}/R > 0.01$.

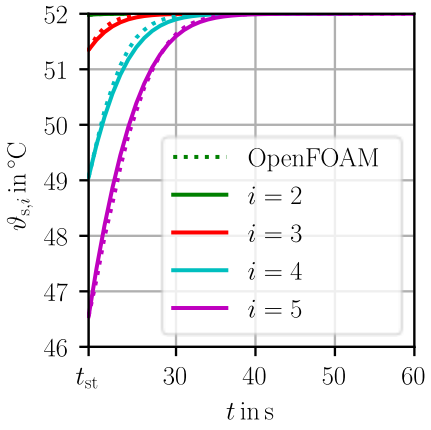

Fig. 10. Comparison of present results to a resolved OpenFOAM simulation from in terms of evolution of soil temperature $\vartheta_{s,i}$ over time under non-isothermal conditions, $t_{st} = 19.0$ s. Lines are only drawn where $h_{s,i,OF}/R > 0.01$.

ISOTHERMAL JET CLEANING

Setup

As a third validation case, jet cleaning of a very thin oil layer is considered. The setup corresponds to the one presented by Yeckel and Middleman [36]. A sketch of the setup with definition of all relevant quantities is shown in Fig. 11. It features a vertical pipe with radius r_0 from which water with a temperature of 25 °C is ejected to form a jet. The jet, which has a minimum radius $r_j < r_0$, impinges perpendicularly on a flat plate. A Newtonian oil layer covers the plate.

The time until the flow is established is negligible compared to the time required for cleaning. Hence, the development phase is neglected, and the flow is considered to be steady. In the region of impact, where $r < r_0$, the pressure gradient and shear forces acting on the soil are of the same order of magnitude. The pressure drops rapidly with increasing radius and is negligible for $r > r_j$ [51, 52]. Since the present modeling framework does not account for pressure forces, they are neglected entirely during the validation simulation. As in the previous validation simulation, an analytical solution of the single-phase flow is employed to obtain the hydrodynamic load τ_{hyd}. The following analytical expressions for the shear stress acting on the soil are used [36, 53]

$$\tau(r) = \begin{cases} 0.39\rho_j u_j^2 Re_j^{-0.5}\frac{r}{r_j} & r < r_0, \\ 0.0346\rho_j u_j^2 Re_j^{-0.2}\left(\frac{r}{r_j}\right)^{-0.2} & r_0 \le r < r_+, \\ \frac{36.0\rho_j u_j^2 Re_j^{0.25}\left(\frac{r}{r_j}\right)^{0.25}}{\left(\left(\frac{r}{r_j}\right)^{2.25} + 32.4 Re_j^{0.25}\right)^2} & r > r_+. \end{cases} \quad (15)$$

Here, the jet Reynolds number $Re_j = u_j r_j/\nu_j$ is computed with the maximum jet velocity u_j, the minimum jet radius r_j and the kinematic viscosity of the cleaning fluid, which is $\nu_j = 8.9 \cdot 10^{-7}$ m^2/s. The transition radius, which is the radius where the velocity profile is developed, is $r_+ = 1.84 r_j Re^{1/9}$. Yeckel and Middleman [36] performed experiments varying the maximum jet velocity u_j, the jet radius r_0, the oil viscosity η_s, the initial soil thickness h_s^0, and the disk radius R. The quantity measured was the evolution of the soil height $\bar{h}_s$ over time. The overbar denotes an average over the plate. Rescaling by using the time using $t^* = 0.089\rho_j \nu_j^{0.2} u_j^{1.8} h_s^0 t/(\eta_s R^{1.2})$ and rescaling the height using $\bar{h}_s^* = \bar{h}_s/h_{s,0}$ demonstrated self-similarity and resulted in a collapse of all profiles onto a single profile.

For validation, Run 5 of Table 1 in [36] was simulated, with $u_j = 4.26$ m/s, $r_0 = 0.229$ cm, $\eta_s = 1$ Pa s, $h_s^0 = h_{s,i}^0 = 60$ µm, $R = 3.75$ cm, $r_j = 0.222$ cm, $Re_j = 10600$ using the present model. In that case $t^* = 1$ corresponds to $t \approx 4$ s. The geometry is described by $A_{out,i} = 2\pi i L_{seg} h_{s,i}$, $A_{int,i} = \pi L_{seg}^2 (2i - 1)$, and $m_{s,i} = \rho_s A_{int,i} h_{s,i}$. The length of a segment is $L_{seg} = R/N_{seg}$.

ISBN: 978-0-9984188-3-4; Published online www.heatexchanger-fouling.com

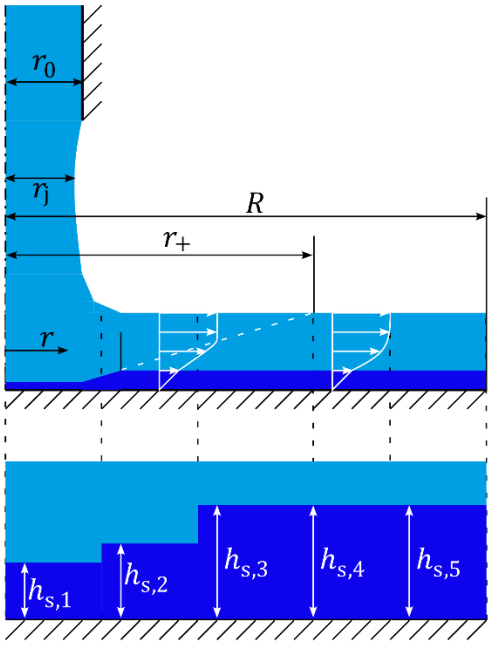

Fig. 11. Setup of the investigated jet cleaning case showing the discretization for $N_{seg} = 5$. The hydraulic jump is not drawn because it occurs further outward at larger radii (picture after [36]).

Results

Finally, results obtained with the present model using $N_{seg} = 5$ for the jet cleaning case are shown in Fig. 12 and compared to experimental data and results obtained with data from the literature. A value of $1/\bar{h}_s^* = 1$ means that the entire soil layer is present, $1/\bar{h}_s^* = 100$ corresponds to 1% of the initial soil.

The present model predicts almost the same results as the model of Yeckel and Middleman [36]. For $t^* \leq 4$ differences up to 40% between the present model and the experiments are observed. The difference might be caused by soil being blasted off by the jet right at the footprint. For $t^* > 4$ the present results agree better with the experimental data. The asymptotic behavior in the region $t^* > 10$ is predicted almost perfectly. Apart from slight differences in the beginning, the present model predicts the same evolution of soil height over time as the model proposed by Yeckel and Middleman [36]. These results validate, again, that the shear stress causes the removal of the thin soil layer. No further quantitative comparison was possible since the exact data were not available.

CONCLUSION

In this paper, a BCCM for the cleaning mechanism viscous shifting was presented. Compared to the models existing in the literature, the newly proposed model has three significant features: i) geometry-independent formulation ii) decoupling of flow computation and soil removal simulation, iii) providing a first-order approximation for inclusion of non-isothermal scenarios. The model was validated using three cases from the literature: an isothermal flushing process of a pipe, a non-isothermal flushing process in a pipe, and jet cleaning of an oil layer. The results show that the model agrees with the references, achieving root-mean-square-errors below 10%.

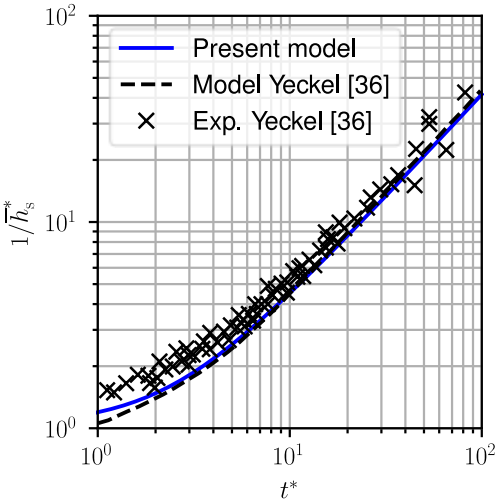

Fig. 12. Comparison of present results to data presented in [36], similar to Fig. 2 from [36].

While the model achieves good results for the cases investigated, it should be noted that the assumptions for the thermal model are very restrictive. In particular, the assumption of adiabatic walls is not given in many practical applications. In general, the temperature development in the soil is coupled with the thermal behavior of the substrate below the soil. To cover this case, at least a one-dimensional, coupled heat conduction problem must be solved. This is the subject of future research, and such a model will be presented in [42]. Another route will be to apply the presented model to more complex soils, like, e.g., petroleum jelly. However, it is questionable whether it is sufficient to consider only the shear forces in these cases. Successful descriptions of viscoplastic soils are possible, for example, using momentum flux per unit width [37] or viscous dissipation [34].

By now, individual models for each cleaning mechanism have been developed. They work well on model soils under constant operating conditions. To account for more realistic and more complex soils, the next step is to develop a combined cleaning model, allowing a transition between the individual models. This provides access to varying operating conditions and more realistic cleaning procedures. The results will be presented in [42].

ISBN: 978-0-9984188-3-4; Published online www.heatexchanger-fouling.com

ACKNOWLEDGEMENTS

This research project is supported by the Industrievereinigung für Lebensmitteltechnologie und Verpackung e.V. (IVLV), the Arbeitsgemeinschaft industrieller Forschungs-vereinigungen „Otto von Guericke“ e.V. (AiF) and the Federal Ministry of Economic Affairs and Climate Action (IGF 21334 BR).

NOMENCLATURE

Latin symbols

A	Area, m^2
$B_{P,1}$	Constant used for thermal fit, $[P]$
$B_{P,2}$	Constant used for thermal fit, ℃
$B_{P,3}$	Constant used for thermal fit, K
c_p	Heat capacity, $\mathrm{J/(kg\,K)}$
H	Enthalpy, J
h_ϑ	Heat convection coefficient, $\mathrm{W/(m^2K)}$
h	Height, m
$\bar{h}$	Average height, m
L	Length, m
m	Mass, kg
$\dot{m}$	Mass flow, $\mathrm{kg/s}$
$\boldsymbol{n}$	Normal vector, $-$
N	Number of, $-$
Nu	Nusselt number, $-$
P	Parameter of the Windhab model, $-$
p	Pressure, Pa
$\dot{Q}$	Heat flux, W
R	Radius, m
Re	Reynolds number, $-$
r	Radial coordinate, m
r_j	Minimum jet radius, m
r_0	Jet exit radius, m
r_+	Transition radius, m
t	Time, s
u	Flow velocity, $\mathrm{m/s}$
x	Spatial coordinate, m
y	Wall normal coordinate, m
z	Spatial coordinate, m

Greek symbols

α	Phase indicator, $-$
$\dot{\gamma}$	Shear rate, $1/\mathrm{s}$
$\dot{\gamma}_\mathrm{ref}$	Parameter of the Windhab model, $1/\mathrm{s}$
Δt	Time step, s
ε_rms	Root-mean-squared error, $-$
η	Dynamic viscosity, Pa s
η_∞	Parameter of the Windhab model, Pa s
κ	Heat conduction coefficient, $\mathrm{W/(m\,K)}$
ν	Kinematic viscosity, $\mathrm{m^2/s}$
ρ	Density, $\mathrm{kg/m^3}$
ϑ	Temperature, ℃
$\boldsymbol{\tau}$	Shear stress tensor, Pa
τ	Shear stress, Pa
τ_hyd	Hydrodynamic load, Pa
τ_0	Parameter of the Windhab model, Pa
τ_1	Parameter of the Windhab model, Pa

Sub- and superscripts

av	Averaging
b	Bulk
chr	Characteristic
f	Fluid, cleaning fluid
fi	Film
i	Index for spatial discretization
in	In
int	Interfacial
j	Jet
max	Maximum
n	Index for temporal discretization
OF	OpenFOAM
P	Parameter
out	Out
s	Soil
seg	Segments
st	Start
$*$	Dimensionless

Abbreviations

BCCM	Boundary condition cleaning model
CFD	Computational fluid dynamics
J	Jet
P	Pipe
VOF	Volume of fluid

REFERENCES

[1] Mickaily, E. S., and Middleman, S., Hydrodynamic cleaning of a viscous film from the inside of a long tube, *AIChE Journal*, vol. 39, pp. 885–893, 1993.

[2] Wilson, D. I., Challenges in Cleaning: Recent Developments and Future Prospects, *Heat Transfer Engineering*, vol. 26, pp. 51–59, 2005.

[3] Palabiyik, I., Lopez-Quiroga, E., Robbins, P. T., Goode, K. R., and Fryer, P. J., Removal of yield-stress fluids from pipework using water, *AIChE Journal*, vol. 64, pp. 1517–1527, 2018.

[4] Landel, J. R., and Wilson, D. I., The fluid mechanics of cleaning and decontamination of surfaces, *Annual Review of Fluid Mechanics*, vol. 53, pp. 147–171, 2021.

[5] Tamime, A. Y., *Cleaning-in place: dairy, food and beverage operations*, 3rd ed., Blackwell Pub, Oxford, UK 2008.

[6] Gésan-Guiziou, G., Sobańtka, A. P., Omont, S., Froelich, D., Rabiller-Baudry, M., Thueux, F., Beudon, D., Tregret, L., Buson, C., and Auffret, D., Life Cycle Assessment of a milk protein fractionation process: Contribution of the production and the cleaning stages at unit process level, *Separation and Purification Technology*, vol. 224, pp. 591–610, 2019.

[7] Köhler, H., Liebmann, V., Golla, C., Fröhlich, J., and Rüdiger, F., Modeling and CFD-simulation of cleaning process for adhesively detaching film-like soils with respect to

ISBN: 978-0-9984188-3-4; Published online www.heatexchanger-fouling.com

industrial application, *Food and Bioproducts Processing*, vol. 129, pp. 157–167, 2021.

[8] Joppa, M., Köhler, H., Rüdiger, F., Majschak, J.-P., and Fröhlich, J., Experiments and simulations on the cleaning of a swellable soil in plane channel flow, *Heat Transfer Engineering*, vol. 38, pp. 786–795, 2017.

[9] Golla, C., Boddin, L., Helbig, M., Köhler, H., Rudiger, F., and Fröhlich, J., Investigating the cleaning mechanism of film-like soils using fully convolutional networks, *Food and Bioproducts Processing*, 2024.

[10] Köhler, H., Liebmann, V., Joppa, M., Fröhlich, J., Majschak, J.-P., and Rüdiger, F., On the Concept of Computational Fluid Dynamics-Based Prediction of Cleaning for Film-Like Soils, *Heat Transfer Engineering*, vol. 43, pp. 1406–1415, 2022.

[11] Golla, C., Köhler, H., Fröhlich, J., and Rüdiger, F., Numerical modeling of a cohesively separating soil layer in consideration of locally varying soil distribution, *Heat and Mass Transfer*, 2023.

[12] Golla, C., Köhler, H., Liebmann, V., Fröhlich, J., and Rüdiger, F., CFD-based three-dimensional modeling of an adhesively detaching soil layer in a channel flow with sudden expansion, *Food and Bioproducts Processing*, vol. 136, pp. 176–183, 2022.

[13] Joppa, M., Köhler, H., Kricke, S., Majschak, J.-P., Fröhlich, J., and Rüdiger, F., Simulation of jet cleaning: diffusion model for swellable soils, *Food and Bioproducts Processing*, vol. 113, pp. 168–176, 2019.

[14] Joppa, M., Köhler, H., Rüdiger, F., Majschak, J.-P., and Fröhlich, J., Prediction of cleaning by means of computational fluid dynamics: implication of the pre-wetting of a swellable soil, *Heat Transfer Engineering*, vol. 41, pp. 178–188, 2020.

[15] Joppa, M., Hanisch, T., and Mauermann, M., Methodology for the assessment of cleanability and geometry optimization using flow simulation on the example of dimple-structured pipe surfaces, *Food and Bioproducts Processing*, vol. 132, pp. 141–154, 2022.

[16] Welchner, K., Zum Ausspülverhalten hochviskoser Produkte aus Rohrleitungen - Wechselwirkungen zwischen Produkt und Spülfluid, Ph.D. thesis, Technische Universität München, Munich, Germany, 1993.

[17] Bhagat, R. K., Perera, A. M., and Wilson, D. I., Cleaning vessel walls by moving water jets: Simple models and supporting experiments, *Food and Bioproducts Processing*, vol. 102, pp. 31–54, 2017.

[18] Aziz, N. A., Zhao, Q., and Fryer, P. J., Visualization on removal mechanisms of food deposit on the modified surfaces, *International Journal of Engineering and Technology*, vol. 4, pp. 31–35, 2007.

[19] Deshmukh, K. P., Arlov, D., Cant, R. S., Göransson, A., Innings, F., and Wilson, D. I., Cleaning of simple cohesive soil layers in a radial flow cell, *Food and Bioproducts Processing*, vol. 136, pp. 84–96, 2022.

[20] Golla, C., Marschall, W. F., Kricke, S., Rüdiger, F., Köhler, H., and Fröhlich, J., Identification of cleaning mechanism by using neural networks, *Food and Bioproducts Processing*, vol. 138, pp. 86–102, 2023.

[21] Liebmann, V., Heide, M., Köhler, H., Rüdiger, F., and Fröhlich, J., Improving flushing processes through targeted control of the temperature boundary conditions, *Proceedings in Applied Mathematics and Mechanics*, vol. 23, pp. e202300253, 2023.

[22] Cole, P. A., Asteriadou, K., Robbins, P. T., Owen, E. G., Montague, G. A., and Fryer, P. J., Comparison of cleaning of toothpaste from surfaces and pilot scale pipework, *Food and Bioproducts Processing*, vol. 88, pp. 392–400, 2010.

[23] Gabard, C., and Hulin, J.-P., Miscible displacement of non-Newtonian fluids in a vertical tube, *The European Physical Journal E*, vol. 11, pp. 231–241, 2003.

[24] Kuang, J., Maxworthy, T., and Petitjeans, P., Miscible displacements between silicone oils in capillary tubes, *European Journal of Mechanics - B/Fluids*, vol. 22, pp. 271–277, 2003.

[25] Park, C., Baek, S., Lee, K., and Kim, S. W., Two-phase flow in a gas-injected capillary tube, *Advances in Polymer Technology*, vol. 22, pp. 320–328, 2003.

[26] Petitjeans, P., and Maxworthy, T., Miscible displacements in capillary tubes. Part 1. Experiments, *Journal of Fluid Mechanics*, vol. 326, pp. 37–56, 1996.

[27] Hasnain, A., Segura, E., and Alba, K., Buoyant displacement flow of immiscible fluids in inclined pipes, *Journal of Fluid Mechanics*, vol. 824, pp. 661–687, 2017.

[28] Oladosu, O., Bhakta, J., and Alba, K., Density-stable yield-stress displacement flow of immiscible fluids in inclined pipes, *Journal of Non-Newtonian Fluid Mechanics*, vol. 275, pp. 104203, 2020.

[29] Swain, P. A. P., Karapetsas, G., Matar, O. K., and Sahu, K. C., Numerical simulation of pressure-driven displacement of a viscoplastic material by a Newtonian fluid using the lattice Boltzmann method, *European Journal of Mechanics - B/Fluids*, vol. 49, pp. 197–207, 2015.

[30] Yan, J., Sáez, A. E., and Grant, C. S., Removal of oil films from stainless steel

ISBN: 978-0-9984188-3-4; Published online www.heatexchanger-fouling.com

tubes, *AIChE Journal*, vol. 43, pp. 251–259, 1997.

[31] Liebmann, V., Heide, M., Köhler, H., Golla, C., Fröhlich, J., and Rüdiger, F., Reduced cleaning model for highly viscous non-Newtonian fluids in pipelines, *Computer Aided Chemical Engineering*, vol. 52, pp. 325–330, 2023.

[32] Fernandes, R. R., Tan, X. S., Wong, E. J., and Wilson, D. I., Flushing and removal of a viscoplastic fluid from pipes, *Food and Bioproducts Processing*, vol. 135, pp. 143–155, 2022.

[33] Fernandes, R. R., Oevermann, D., and Wilson, D. I., Cleaning insoluble viscoplastic soil layers using static and moving coherent impinging water jets, *Chemical Engineering Science*, vol. 207, pp. 752–768, 2019.

[34] Fernandes, R. R., and Wilson, D. I., Modelling the cleaning of viscoplastic layers by impinging coherent turbulent water jets, *Journal of Non-Newtonian Fluid Mechanics*, vol. 282, pp. 104314, 2020.

[35] Fernandes, R. R., Tsai, J.-H., and Wilson, D. I., Comparison of models for predicting cleaning of viscoplastic soil layers by impinging coherent turbulent water jets, *Chemical Engineering Science*, vol. 248, pp. 117060, 2022.

[36] Yeckel, A., and Middleman, S., Removal of a viscous film from a rigid plane surface by an impinging liquid jet, *Chemical Engineering Communications*, vol. 50, pp. 165–175, 1987.

[37] Glover, H. W., Brass, T., Bhagat, R. K., Davidson, J. F., Pratt, L., and Wilson, D. I., Cleaning of complex soil layers on vertical walls by fixed and moving impinging liquid jets, *Journal of Food Engineering*, vol. 178, pp. 95–109, 2016.

[38] Uth, T., and Deshpande, V. S., Unsteady penetration of a target by a liquid jet, *Proceedings of the National Academy of Sciences*, vol. 110, pp. 20028–20033, 2013.

[39] Toschi, F., and Sega, M. (Eds.), *Flowing Matter*, Springer, Cham, 2019.

[40] Yeckel, A., Middleman, S., and Klumb, L. A., The removal of thin liquid films from periodically grooved surfaces by an impinging jet, *Chemical Engineering Communications*, vol. 96, pp. 69–79, 1990.

[41] Yeckel, A., Strong, L., and Middleman, S., Viscous film flow in the stagnation region of the jet impinging on planar surface, *AIChE Journal*, vol. 40, pp. 1611–1617, 1994.

[42] Golla, C., Jena, S., Liebmann, V., Fröhlich, J., Rüdiger, F., and Köhler, H., A cleaning model for film-like soils with transition between cleaning mechanisms, in: *Proceedings of 15th International Conference on Heat Exchanger Fouling and Cleaning 2024*, Lisbon, Portugal 2024.

[43] Eischen, J.-C., and Windhab, E. J., Viscosity of Cocoa and Chocolate Products, *Applied Rheology*, vol. 12, pp. 32–34, 2002.

[44] Pitsillou, R., Georgiou, G. C., and Huilgol, R. R., On the use of the Lambert function in solving non-Newtonian flow problems, *Physics of Fluids*, vol. 32, pp. 093101, 2020.

[45] Hickox, C. E., Instability due to Viscosity and Density Stratification in Axisymmetric Pipe Flow, *The Physics of Fluids*, vol. 14, pp. 251–262, 1971.

[46] Joseph, D. D., Renardy, M., and Renardy, Y., Instability of the flow of two immiscible liquids with different viscosities in a pipe, *Journal of Fluid Mechanics*, vol. 141, pp. 309–317, 1984.

[47] Preziosi, L., Chen, K., and Joseph, D. D., Lubricated pipelining: stability of core-annular flow, *Journal of Fluid Mechanics*, vol. 201, pp. 323, 1989.

[48] Papageorgiou, D. T., Maldarelli, C., and Rumschitzki, D. S., Nonlinear interfacial stability of core-annular film flows, *Physics of Fluids A: Fluid Dynamics*, vol. 2, pp. 340–352, 1990.

[49] Hu, H. H., and Joseph, D. D., Lubricated pipelining: stability of core-annular flow. Part 2, *Journal of Fluid Mechanics*, vol. 205, pp. 359, 1989.

[50] Baehr, H. D., and Stephan, K., *Heat and mass-transfer*, 2nd rev. ed, Springer, Berlin New York 2006.

[51] Nakoryakov, V. E., Pokusaev, B. G., and Troyan, E. N., Impingement of an axisymmetric liquid jet on a barrier, *International Journal of Heat and Mass Transfer*, vol. 21, pp. 1175–1184, 1978.

[52] Scholtz, M. T., and Trass, O., Mass transfer in a nonuniform impinging jet: Part I. Stagnation flow-velocity and pressure distribution, *AIChE Journal*, vol. 16, pp. 82–90, 1970.

[53] Watson, E. J., The radial spread of a liquid jet over a horizontal plane, *Journal of Fluid Mechanics*, vol. 20, pp. 481–499, 1964.

ISBN: 978-0-9984188-3-4; Published online www.heatexchanger-fouling.com